THE ASTROPHYSICAL JOURNAL, 466:768–778, 1996 August 1

A SHOCK EMISSION MODEL FOR GAMMA-RAY BURSTS. II. SPECTRAL PROPERTIES

M. TAVANI
Columbia Astrophysics Laboratory, Columbia University, New York, NY 10027
Received 1995 July 26; accepted 1996 January 22

ABSTRACT

We discuss a simple model of high-energy emission for gamma-ray bursts (GRBs) based on synchrotron radiation of particles impulsively accelerated. The emission model assumes a source of magnetohydrodynamical outflow and efficient and fast particle acceleration (most likely mediated by a relativistic shock) in optically thin environments. The properties of the synchrotron shock emission can be derived under general conditions valid for both Galactic or cosmological interpretations of GRB sources. We show that the synchrotron shock model (SSM) predicts a specific shape of the GRB spectral continuum (broad maximum of the νF_ν spectrum, low-energy continuum with characteristic curvature, high-energy power-law emission) in agreement with recently determined broadband GRB spectra. The calculated spectrum turns out to be a universal two-parameter function in the energy range ~ 30 keV–1 GeV. The peak photon energy E_p of the GRB νF_ν spectrum (power per logarithmic photon energy band) is interpreted as the relativistic synchrotron energy of impulsively accelerated particles. From the GRB properties, we obtain a crucial constraint relating the average Lorentz factor of preaccelerated particles γ_* and the strength of the local magnetic field $B_{\rm ps}$ at the GRB site (modulo possible Doppler and cosmological factors of order $\sim 10^2$ and an inverse Compton blueshift factor):

$$10^{12} \lesssim \gamma_*^2 B_{\rm ps} \lesssim 10^{14} \text{ cgs} .$$

Hard-to-soft spectral evolution often observed in GRBs can be due to a variation of γ_* and $B_{\rm ps}$ as the synchrotron emission evolves within the burst. The burst emissivity depends on the strength of the average magnetic field at the acceleration site, and we derive general relations from among peak intensities, durations, and E_p's of elementary shock emission episodes. In general, a complex burst can be a superposition of different elementary shock emission episodes, and the durations of elementary shock emission episodes τ_e can tentatively be identified with those of individual GRB pulses. We find that the pulse durations τ_e have a simple physical meaning. On the contrary, the statistically defined durations T_{90} and T_{50} are not suitable for an accurate description of GRB physical processes.

The SSM in its simplest realization predicts correlated spectral hardness and burst intensity and an anticorrelation between shock episode durations τ_e and peak intensities. Both of these characteristics are qualitatively similar to GRB features expected in cosmological models.

The determination of the GRB spectral continuum shapes as a function of time is particularly important for testing the shock model proposed here. Under general conditions of emission, the SSM predicts specific patterns of spectral evolution which can be tested. In this paper, we discuss the general properties of the shock emission model, and we leave open the issue of the ultimate origin of the relativistic MHD winds and nature of the outbursts.

Subject headings: gamma rays: bursts — gamma rays: theory — radiation mechanisms: nonthermal — shock waves

1. INTRODUCTION

The nature of gamma-ray bursts (GRBs) remains elusive despite recent observational and theoretical investigations. The spatial isotropic and inhomogeneous distribution of GRBs revealed by the BATSE instruments on board the *Compton Gamma-Ray Observatory* (*CGRO*) (e.g., Fishman et al. 1994, hereafter F94; Meegan et al. 1992, 1996) cannot be reconciled with a population of sources concentrated in the Galactic plane. In principle, three distance scales have been proposed, involving the heliospheric contact discontinuity at $\sim 10^3$ AU, a Galactic halo distance at ~ 100 kpc (e.g., Hakkila et al. 1994), or an extragalactic distance scale at $\gtrsim 200\, h^{-1}$ Mpc, with h the Hubble constant in units of 100 km s^{-1} Mpc^{-1} (Paczyński 1990; Shemi & Piran 1990; Rees & Mészáros 1992; Narayan, Paczyński, & Piran 1992; Mészáros & Rees 1993; Mészáros et al. 1993; Mészáros, Rees, & Papathanassiou 1994; Hartmann, Briggs, & Mannheim 1996)

In this paper we discuss the spectral properties of an emission mechanism characteristic of relativistic shocks in optically thin environments. A way to avoid photon energy degradation and electron-positron ($e^\pm$) pair creation following a GRB event is to induce a situation where the bulk of

the GRB total energy is first transformed into a relativistic electromagnetic/particle plasma outflow and then radiated by a shock mechanism (e.g., Mészáros et al. 1993; Tavani 1995, 1996a). Shock models were recently proposed mainly in the context of an extragalactic origin of GRBs (Rees & Mészáros 1992; Mészáros & Rees 1993; Mészáros et al. 1993, 1994). However, the physical mechanism of high-energy emission from relativistic shocks has general validity, and it can be applied to both extragalactic and Galactic models of GRBs (Tavani 1995, 1996a). The point of view adopted in this paper is therefore to provide a general computational framework of spectral and temporal properties of GRBs within the context of relativistic shock models.

We leave open in this paper the issue of determining the class of astrophysical sources producing the GRB phenomenon. Conventional or unconventional compact star sources can be invoked to justify the energetics and the characteristics of the relativistic shock emission considered here. Relativistic winds are an ubiquitous characteristic of compact objects producing energetic outflows. Examples include collimated outflows from active galactic nuclei (e.g., Begelman, Blandford, & Rees 1984), plasmoid ejection from Galactic superluminal X-ray transients following major accretion episodes (e.g., Mirabel & Rodriguez 1994; Hjellming & Rupen 1995), relativistic winds from radio pulsars (e.g., Kennel & Coroniti 1984; Hester et al. 1995), and possibly outflows related to the outbursting activity of soft gamma-ray repeaters (Tavani 1994). These particle/electromagnetic outflows are likely to be produced and accelerated by MHD processes, and asymptotically thermalized outflows (in the comoving frame of the flow) with bulk relativistic speeds can be achieved (e.g., Chiueh, Li, & Begelman 1991). The precise nature of the class of compact objects related to GRBs is irrelevant for a shock emission process occurring at large distance from their sources. We focus here on the modeling of the main and most energetic component of the GRB emission in the energy range ~ 30 keV–500 MeV (Fishman et al. 1994; Schaefer et al. 1994a, b; Hanlon et al. 1994; Winkler et al. 1995; Hurley et al. 1994). In what follows, we neglect other (less energetic) *additional* spectral components occasionally detected from GRBs, such as, e.g., X-ray precursors and extended emissions (Murakami et al. 1991), an additional soft X-ray component detected by BATSE in $\sim 15\%$ of GRBs (Preece et al. 1995), and the gamma-ray "delayed" emission (Sommer et al. 1994; Hurley et al. 1994).

We present in § 2 the main features of the shock emission model applied in its generality to GRBs. The main spectral and temporal characteristics of the model are discussed in § 3, and a comparison with observed spectra of bright GRBs is presented in § 4. We briefly discuss future tests in § 5 and summarize our conclusions in § 6. A more general treatment of the physical processes occurring in relativistic shocks for cosmological or Galactic models of GRBs will appear elsewhere. A short account of the main features of the GRB shock emission model was presented in Tavani (1996a).

2. A GRB SHOCK EMISSION MODEL

Let us assume a central outbursting source surrounded by an optically thin nebular medium which can be gaseous material self-generated by the GRB source, a low-density interstellar medium (ISM), a supernova remnant (SNR), or a gaseous environment provided by a mass outflow from a companion star in a binary system. A relativistic wind is assumed to be produced by a compact star source because of a major impulsive event. An MHD relativistic wind is a mixture of electromagnetic fields, $e^{\pm}$-pairs, and baryons. In general, it can be parametrized by a bulk Lorentz factor Γ, by an internal Lorentz factor γ_* (if a mechanism internal to the MHD flow, e.g., electromagnetic wave acceleration of pulsar relativistic winds or internal shocks, accelerates particles in the comoving frame), by an MHD ratio of average comoving electromagnetic and particle kinetic energy densities or wind "magnetization" $\sigma_M = (B_w^2/4\pi)/\mathscr{E}_K$ (with B_w the magnetic field strength and $\mathscr{E}_K$ the total particle kinetic energy density in the comoving frame), and by $\xi = n_b/n_{\pm}$, the comoving ratio of total baryonic number density n_b to the $e^{\pm}$-pair number density $n_{\pm}$. A shock front develops in the surrounding medium as a hydrodynamical response to the MHD wave and particle energy sweeping the medium. Forward (in the medium) and reverse (in the MHD ejecta) shocks develop typically as the kinetic energy of the swept-up material approaches the initial outflow kinetic energy for a moving shock front not in pressure equilibrium (e.g., Rees & Mészáros 1992). Alternately, a (binary) nebular environment can determine a quasi-static shock radius. The relativistic emission processes at the shock front are particularly important for the reverse shock, and we will concentrate mostly on the radiative properties of the shock affecting the MHD wind. In the following, we denote by "shock front" the MHD reverse shock front affecting the burst ejecta.

If the relativistic wind interacts with a nebular environment not in pressure equilibrium with the outflow, the relativistic motion of the resulting shock front is characterized by a bulk Lorentz factor Γ. On the other hand, if the shock front is in pressure equilibrium with the MHD outflow, a static shock front ensues, and the following formulae are valid with the substitution $\Gamma = 1$. For a static shock, the emitted photon energies E and burst durations τ_b are independent of the Lorentz bulk factor Γ. Alternately, as a second extreme case, a shock front moving directly toward the observer (assumed in cosmological models; see Mészáros & Rees 1993; Mészáros et al. 1993, 1994) produces blueshifted photon energies in the laboratory frame, $E = \Gamma E'$, and a decrease in the observed burst dynamical timescale $\tau_d = \tau_d'/\Gamma^2$, where the primed quantities refer to the shock front rest frame (e.g., Mészáros & Rees 1993).

The flow can be idealized as being confined within a cone of radial length R_s (the shock radius) and a half-opening angle at the source, $\theta = 10^{-1}\theta_{-1}$ (for isotropic emission, $\theta_{-1} = 10$), sweeping a volume in the laboratory frame of width $\delta l = \delta l_{10}$ (10^{10} cm). The energy density at the shock radius R_s is, e.g., $\mathscr{E}(R_s) \sim (10 \text{ ergs cm}^{-3})$ $R_{s,16}^{-2}\delta l_{10}^{-1}E_{b,42}\theta_{-1}^{-2}\epsilon_r^{-1}$, where we defined $R_s = R_{s,16} \times 10^{16}$ cm, with $E_{b,42} = E_{b,42} \times 10^{42}$ ergs the outburst radiated energy, and ϵ_r the radiative efficiency of the burst. For cosmological models of GRBs, proper values of E_b and δl need to be adopted (e.g., Mészáros & Rees 1993; Mészáros et al. 1993). The equipartition magnetic field of the outflow at the shock is $B_e(R_s) \sim (16 \text{ G})$ $R_{s,16}^{-1}\theta_{-1}^{-1}(E_{b,42}/\delta l_{10}E_b)^{1/2}$, and the effective magnetic field shock-enhanced and modified by the MHD magnetization is $B_{ps}(R_s) = 3B_e(R_s)[2\sigma_M/(1+\sigma_M)]^{1/2}$ (e.g., Kennel &

Coroniti 1984). The dynamical timescale of relativistic expansion in the comoving frame is $\tau'_d \simeq R_s/c$, and it might determine the relevant timescale of burst emission for a particular class of GRB models (Mészáros, Laguna, & Rees 1993). More generally, time variability of the GRB emission is established by the several effects including dynamical expansion, interaction with the surrounding medium, and radiative cooling (synchrotron emission and inverse Compton).

Initially, before the relativistic MHD plasma interacts with a shock front, the particle distribution function is assumed to be completely thermalized and characterized by a single (relativistic) particle energy or temperature. The thermal nature of the asymptotic energy distribution of particles in MHD outflows is established by the relatively short MHD interaction timescale (relating particles and comoving electromagnetic fields) compared to typical dynamical timescales necessary to reach the interaction shock radius (e.g., Chiueh et al. 1991). Depending on the strength and on the spatial ordering of the magnetic field at the shock, the preshock (and postshock) particle distribution function can be two-dimensional or three-dimensional. A disordered and possibly turbulent magnetic field at the shock is likely to isotropize any distribution function, and in the following we will assume the simplest case of a randomly ordered magnetic field with no preferred direction with respect to the line of sight. Three-dimensional distribution giving the radiating particle number per energy interval $d\gamma$ and solid angle $d\Omega$ is properly described by a relativistic Maxwellian[1] distribution (e.g., Jones & Hardee 1979):

$$n_{\rm th}^{(3D)}(\gamma, \alpha) d\gamma\, d\Omega = \frac{N_{\pm}^{M}}{8\pi} \frac{\gamma^2}{\gamma_*^3} e^{-\gamma/\gamma_*} d\gamma\, d\Omega\,, \qquad (1)$$

where $\gamma = E_{\pm}/m_{\pm}c^2$, $\gamma_* = k_{\rm B}T^*/m_{\pm}c^2$, with T^* the preshock distribution temperature of radiating particles (electrons and positrons, if present, of mass $m_{\pm}$) of energy $E_{\pm}$, $k_{\rm B}$ the Boltzmann constant, and c the speed of light, $d\Omega = d\cos\alpha\, d\phi$ the solid angle with α the pitch angle of the particle trajectory with respect to the local magnetic field direction, ϕ the azimuthal angle, and $N_{\pm}^{M}$ a normalization constant.

Acceleration processes can take place at a shock front or in an environment subject to strong magnetic field turbulence. As a consequence, the postacceleration particle energy distribution function can be drastically altered by the formation of a suprathermal component. This suprathermal component is a nontrivial function of the particle and relativistic structure of the MHD outflow as well as of the shock acceleration mechanism. Acceleration shock theory is poorly constrained in the relativistic regime (e.g., Jones & Ellison 1991), and we need to consider several possible mechanisms. Diffusive acceleration for a local magnetic field mostly parallel to the shock front can operate within a factor of $\sim$10–100 of the timescale $R_{\rm L}/c$ (with $R_{\rm L}$ the Larmor radius of the accelerated particles). Alternately, for a local magnetic field mostly perpendicular to the shock normal, acceleration by magnetosonic waves mediated by the presence of ions (e.g., Arons 1991) or by a shock-drift mechanism (e.g., Begelman & Kirk 1990) can occur.[2] The altered postshock distribution function with a suprathermal power-law tail of index δ (we omit the solid angle and energy differential $d\gamma d\Omega$) can be written as:

$$n_{\rm ps}^{(3D)}(\gamma, \alpha) = \frac{f_\alpha N_{\pm}}{4\pi}\left[\left(\frac{\gamma^2}{\gamma_*^3} e^{-\gamma/\gamma_*}\right) + \mathscr{C}\left(\frac{\gamma}{\gamma_*}\right)^{-\delta}\right], \qquad (2)$$

where $N_{\pm}$ and $\mathscr{C}$ are appropriate normalization constants, and f_α takes into account the possible spatial nonuniformity of the pitch angle distribution with respect to the pitch angle. The energy range of the power-law distribution is $\gamma_* \le \gamma \le \gamma_m$, where γ_m is a maximum energy of shock-accelerated particles. The maximum Lorentz factor γ_m is to be determined by balancing acceleration and cooling losses in the shock comoving frame. Efficient shock acceleration requires in general that the acceleration timescale τ'_a satisfies the condition $\tau'_a \lesssim \tau'_r$, with the radiating timescale τ'_r satisfying the relation $\tau_r'^{-1} = \tau_s'^{-1} + \tau_{\rm IC}'^{-1}$, where τ'_s and $\tau'_{\rm IC}$ are the comoving synchrotron and IC radiation timescales, respectively. Furthermore, the constant $\mathscr{C}$ is strongly dependent on the geometric and radiative conditions of the acceleration site.

We find that a very efficient acceleration process drives the GRB process. For *maximally efficient shock acceleration* (as theoretically and observationally derived in relativistic MHD shock models of high-energy emission from SNR and binary plerions, e.g., Hoshino et al. 1992; Tavani & Arons 1996) a simple condition for $\mathscr{C}$ can be derived, i.e., $\mathscr{C} = 1/(e\gamma_*)$.

The physical meaning of equation (2) with the maximally efficient acceleration condition imposed on $\mathscr{C}$ (that we assume in the following) is clear. The resulting particle energy distribution of initial average energy γ_* and thermal low-energy tail (as produced by rapid thermalization processes during the MHD preacceleration expansion or at the shock site) is modified at the top of the distribution for $\gamma = \gamma_*$ by a suprathermal power-law component resulting from fast acceleration. Note that the degree of applicability of equation (2) depends on the efficiency of particle acceleration and subsequent radiative (and possible adiabatic) cooling influencing the particle distribution. The condition $\tau'_a \lesssim \tau'_r$ is the crucial requirement for a physical mechanism of emission that makes possible a suprathermal component in GRB spectra.

Synchrotron radiation and inverse Compton scattering dominate the emission of shocked radiating particles, and the ratio of comoving energy densities $\mathscr{E}'_M/\mathscr{E}'_R$ (with $\mathscr{E}'_M$ and $\mathscr{E}'_R$ the magnetic and radiation energy densities,

[1] A calculation for a two-dimensional distribution of particles confined in a plane perpendicular to the direction of an ordered magnetic field gives results similar to those reported here.

[2] Shock acceleration models are characterized by acceleration timescales that may drastically differ from one model to the other. The acceleration timescale in the comoving frame of the shock front τ'_a is generally related to the inverse of the relativistic cyclotron frequency driving the acceleration, i.e., $\tau'_a \sim \Omega_e^{-1}$ or $\tau'_a \sim \Omega_i^{-1}$, with $\Omega_e = eB_s/\gamma m_{\pm}c$ and $\Omega_i = eB_s/\gamma m_i c$, the relativistic $e^{\pm}$-pair and ion (of mass m_i) cyclotron frequencies, respectively. Also the maximum particle energy E_m of the postshock accelerated distribution is model dependent, and it may be further limited by strong radiative losses such as synchrotron and inverse Compton (IC) losses. As an example, observed shock-driven E_m are in the $\gtrsim$TeV range for static or quasi-static shocks of pulsar-driven nebulae such as the Crab nebula (Kennel & Coroniti 1984) and the binary plerion PSR 1259−63 (Tavani & Arons 1996). The smallest acceleration timescale of relativistic MHD shocks was recently determined for the PSR 1259−63 system near periastron, with τ_a reaching values less than $\sim 10^2$–10^3 s (Tavani & Arons 1996). Ultimately, as we will discuss in § 3, GRB phenomena may constrain impulsive acceleration mechanisms in a radiative regime not easily accessible in other astrophysical sources.

respectively) determines the relative importance of the two emission mechanisms. In the absence of an external source of soft photons, the (self-) inverse Compton (IC) contribution to the radiated flux originates from the low-energy synchrotron photons upscattered by the relativistic population of postshock $e^{\pm}$-pairs. In the following, we consider an emission model for which synchrotron emission determines the GRB spectral continuum. Even though in principle IC can play a major role in shaping the GRB spectral continuum (e.g., Mészáros et al. 1994), we assume in the following that IC scattering does not drastically alter the *spectral shape* of the GRB emission. We refer to this approximation as the synchrotron shock model (SSM).

The synchrotron spectral energy emissivity per unit volume and solid angle $J^s_\nu(\alpha)$ is therefore

$$J^s_\nu(\alpha) = \int_1^\infty p^s_\nu(\gamma, \alpha) n^{(3D)}_{ps}(\gamma, \alpha) d\gamma = \left(\frac{3^{1/2}}{16\pi^2}\right)\left(\frac{N_\pm}{c_2}\right)\left(\frac{q'^3}{m_\pm c^2}\right) f_\alpha B_{ps} \sin\alpha \left[\mathscr{F}\left(\frac{\nu}{\nu^*_c \sin\alpha}\right)\right], \quad (3)$$

with $\nu^*_c \equiv (3/4\pi)(q' B_{ps}/m_\pm c)\gamma^2_*$ the critical frequency corresponding to the preshock temperature γ_* of particles of charge e', $p^s_\nu(\gamma, \alpha)$ the single-particle synchrotron power, $N_\pm$ the local $q^\pm$-pair number density, c_2 a normalization constant, viz., $c_2 = 2 - 5/e + [1 - y_m^{1-\delta}]/[e(\delta - 1)]$, and $\mathscr{F}(w)$ a dimensionless spectral function given by (Tavani 1996a)

$$\mathscr{F}(w) \equiv \int_0^1 y^2 e^{-y} F'\left(\frac{w}{y^2}\right) dy + \frac{1}{e}\int_1^{y_m} y^{-\delta} F'\left(\frac{w}{y^2}\right) dy , \quad (4)$$

where we defined

$$w = \nu/(\nu^*_c \sin\alpha) , \quad y = \gamma/\gamma_* , \quad y_m = \gamma_m/\gamma_* \quad (5)$$

with

$$F'(x) \equiv x\int_x^\infty K_{5/3}(x') dx' \quad (6)$$

the synchrotron spectral function, and $K_{5/3}(x')$ the modified Bessel function of order 5/3 (e.g., Pacholczyk 1969). The differential proper intensity in the shock comoving frame (proper intensity) I^s_ν is obtained after an integration of J^s_ν over the solid angle $d\Omega(\alpha)$ and emission volume dV

$$I^s_\nu = \iint J^s_\nu(\alpha) d\Omega(\alpha) dV . \quad (7)$$

The observed spectral flux F^s_ν can be obtained from the proper intensity I^s_ν by dividing by the square of the source distance D, and by taking into account the possible effects of relativistic beaming and possible cosmological effects. Relativistic beaming of radiation produced in a moving shock front leads to

$$F^s_\nu(\Gamma, i, D) = \frac{1}{4\pi D^2}[\mathscr{D}(\Gamma, i)]^3 I^s_{\nu/\mathscr{D}} , \quad (8)$$

where $\mathscr{D}(\Gamma, \theta)$ is the relativistic Doppler boost coefficient

$$\mathscr{D}(\Gamma, i) = \frac{1}{\Gamma[1 - \boldsymbol{\beta}\cdot\boldsymbol{\mu}(i)]} , \quad (9)$$

with i the angle between the line of sight and the boosting direction, $\boldsymbol{\mu}(i)$ the direction cosines with origin on the source, $\boldsymbol{\beta}$ the velocity vector of the moving shock, and $\Gamma = (1 - \beta^2)^{-1/2}$, where $\beta = |\boldsymbol{\beta}|$. For a small angle $i \sim 1/\Gamma$ (as assumed in cosmological models of GRBs, e.g., Mészáros et al. 1993), we have $\mathscr{D}(\Gamma, 1/\Gamma) \sim 2\Gamma$. Note, however, that for generic inclination angles, equations (8)–(9) should be used. In general, different shock emission episodes may originate from different sites differing by their Doppler boost coefficients $\mathscr{D}(\Gamma, i)$. Obviously, for a standing shock, the expression for F^s_ν simplifies to $F^s_\nu(D) = (1/4\pi D^2) I^s_\nu$. For GRBs at cosmological distances, both the observed frequency and distance change into

$$\nu \to \nu'' = (1 + z)\nu ,$$
$$D \to D'' = \frac{c}{H_0}\frac{1}{(1 + z)q_0^2} \times [1 - q_0 + q_0 z + (q_0 - 1)\sqrt{1 + 2q_0 z}] , \quad (10)$$

where z is the cosmological redshift, D'' the luminosity distance of a simple cosmological model with zero curvature and cosmological constant, q_0 the deceleration parameter, and H_0 the Hubble constant. The function F^s_ν may therefore be dependent on the additional parameter z and in general,

$$F^s_\nu(\Gamma, i, D, z) = F^s_{(1+z)\nu}(\Gamma, i, D'')/(1 + z)^2 , \quad (11)$$

with the observed frequency ν depending on the emitted frequency ν' as $\nu = [\mathscr{D}(\Gamma, i)/(1 + z)]\nu'$. In the following, we will use the shortened expression F^s_ν for the general expression of equation (11).

For an isotropic pitch angle distribution and/or randomized directions of the magnetic field at the shock front ($f_\alpha = 1$), we obtain from equations (3)–(4) the important and simple relation that determines the *spectral* flux of SSM:

$$F^s_\nu \propto B_{ps}\mathscr{F}(\nu/\nu^*_c) . \quad (12)$$

Equation (12) characterizes the synchrotron shock model of GRB emission in its simplest realization. The observed flux is proportional to the local magnetic field strength at the shock and depends on the emitted photon energy (frequency) through the dimensionless spectral function $\mathscr{F}$. The magnetic field strength at the shock ultimately sets the emitted synchrotron power and the critical energy determining the only clearly discernible spectral feature of the low-energy synchrotron spectrum, i.e., the peak energy E_p corresponding to the synchrotron frequency ν^*_c (modulo possible Doppler, IC, and cosmological redshift factors). It is important to notice that the SSM function F^s_ν also depends on the emission volume V and number density $N_\pm$. For the simple assumption of similar emission volumes V and values of $N_\pm$ for all GRBs, differences in GRB peak intensities can be related to different magnetic field strengths at the emission sites, a condition that can be tested by the study of correlated behavior of peak intensities, E_p, and shock episode durations, as we will discuss in the next section.

We also note that for an isotropic pitch angle distribution the synchrotron timescale in the comoving shock frame is $\tau'_s = 6\pi(m_\pm c/\sigma_T)\gamma_b^{-1} B_{ps}^{-2} \sim (8 \times 10^2 \text{ s}) B_{ps}^{-2}\gamma_{b,6}^{-1}$ (with $\gamma_b = \gamma_{b,6} \times 10^6$ the average Lorentz factor of shocked radiating particles, σ_T the Thomson cross section, and B_{ps} in gauss). The synchrotron timescale τ'_s establishes a fundamental temporal scale of shock emission. GRBs may be superpositions of different shock emission episodes, likely to be identified with the "pulses" of complex GRB light curves. If the observed synchrotron timescale is longer than the

dynamical timescale in the laboratory frame, a fundamental GRB duration scale is set by τ_s' times a possible Doppler and/or cosmological factor. It is important to point out that in general the timescale of synchrotron shock emission should not be confused with the observed average burst durations (e.g., T_{90} or T_{50}) used in schematic representations of GRB temporal properties (e.g., Fishman et al. 1994; Meegan et al. 1996). See § 3 for further discussion of this important point.

3. CHARACTERISTICS OF THE GRB SHOCK EMISSION

We can now proceed to calculate the shock-driven synchrotron spectrum following the simple prescriptions of the previous section. It is convenient to calculate νF_ν as a function of the dimensionless quantity $\zeta = \nu/\nu_c^*$.

We first calculate the synchrotron spectrum in the absence of postshock particle acceleration, i.e., for a relativistic Maxwellian given in equation (1). Figure 1 shows the characteristic spectral shape of the νF_ν for this case. The spectrum is characterized by substantial curvature and by a broad maximum occurring at the peak energy of the νF_ν spectrum in correspondence with the normalized energy $\zeta_{p,\rm th} \simeq 25$. For $\zeta \gtrsim \zeta_{p,\rm th}$, the spectrum decreases exponentially. In any case, the νF_ν is substantially broader than that for blackbody emission (given by the *dashed curve* of Fig. 1). It is important to note that the synchrotron spectrum of a purely relativistic Maxwellian distribution does not fit any of the GRB spectra of Table 1.

Figure 2 shows the calculated synchrotron spectrum for the case dominated by efficient shock acceleration (eqs. [3]–[4]). Figure 2 is obtained for different assumptions about the index of the suprathermal distribution δ in the range likely to be applicable to GRBs, $3.5 \le \delta \le 6.0$.

We find that the normalized peak energy of the νF_ν spectrum with a suprathermal tail is typically a factor of ~ 10 smaller than for the purely Maxwellian case, i.e., $\zeta_{p,\rm st} \simeq 2.5$. The true critical energy E_c can therefore be obtained from the observable peak energy E_p of the νF_ν spectrum as $E_c = E_p/\zeta_p \sim 0.4 E_p$. The low-energy part of the νF_ν spectrum depends on photon frequency as $\nu F_\nu \sim \nu^{4/3}$ (corresponding to a power-law photon index $\alpha = -0.67$; see also Katz 1994), and the power-law behavior is modified near E_p in a very distinctive and parameter-independent way. The high-energy component well above the peak energy can be approximated as $\nu F_\nu \sim \nu^{-(\delta-3)/2}$ corresponding to the usual relation between δ and synchrotron/IC spectral index $\beta = (\delta + 1)/2$. We note that the spectral characteristics of the shock-powered continuum with suprathermal tail (low-energy component with distinctive curvature, peak energy of the νF_ν spectrum, high-energy component) are *uniquely* determined with a universal shape of the continuum at energies below ζ_p.

TABLE 1

CHARACTERISTICS OF COMPOSITE GRB SPECTRA

GRB	E_p[a] (MeV)	Δt[b] (s)	Complexity	$[\mathcal{D}(\Gamma, i)/(1+z)][\gamma_*^2 B_{\rm ps}]_{12}$[c]	δ[c]
910503....	~1.0	~10	Quasi-simple	45	~3.8
910601....	~0.5	~40	Multispiked	30	~6
910814....	~2.0	~14	Quasi-simple	120	~5
920622....	~0.5	~20	Multispiked	30	~5
940217....	~0.6	~160	multispiked	25	~4

[a] Peak photon energy of the νF_ν spectrum. Data from Schaefer et al. 1994a, b, 1995; Hurley et al. 1994; Winkler et al. 1995; Greiner et al. 1995.

[b] Integration times for the composite spectra.

[c] Best-fit parameters of the synchrotron shock emission model, see text for definitions.

Figure 3 gives a comparison between the SSM spectrum (with $\delta = 3.8$ to match the high-energy properties of GRB 910503) and a phenomenological spectral model applied to time-averaged GRB spectra defined as

$$N_E(E) \propto \begin{cases} \left(\dfrac{E}{100\ \rm keV}\right)^{\alpha'} e^{-E/E_0} & \text{for } E \le (\alpha' - \beta')E_0\ , \\ \left(\dfrac{E}{100\ \rm keV}\right)^{\beta'} & \text{for } E \ge (\alpha' - \beta')E_0\ , \end{cases} \tag{13}$$

where E is the photon energy, $N_E(E)$ is the differential photon number per energy decade, E_0 is a "break" energy, and α' and β' (negative) are spectral indices (Band et al. 1993; hereafter B93). An extra normalization constant in

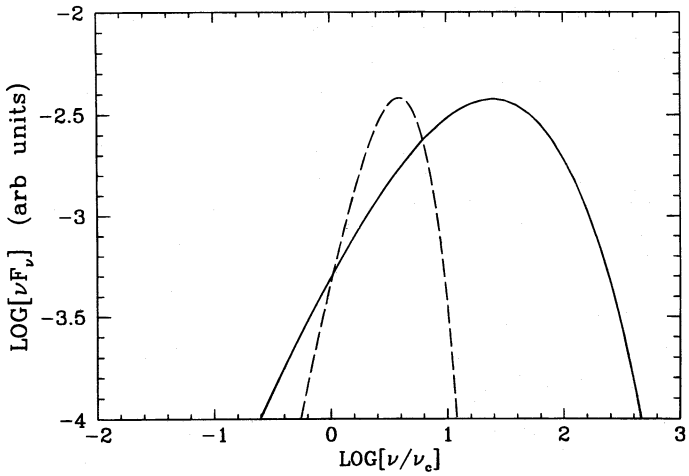

FIG. 1.—*Solid curve:* calculated νF_ν spectrum for a purely Maxwellian postshock particle energy distribution as a function of the dimensionless energy ν/ν_c^*. *Dotted curve:* νF_ν spectrum for blackbody corresponding to a temperature equivalent to ν_c^*.

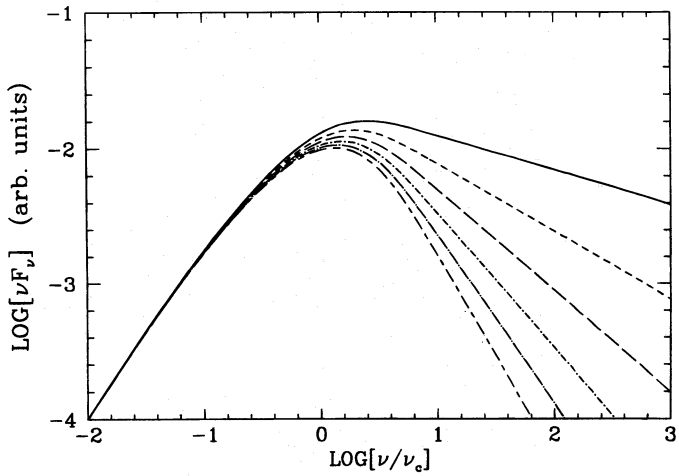

FIG. 2.—Calculated νF_ν spectra for postshock particle distribution functions modified by maximally efficient suprathermal components of different indices δ. *Solid curve:* case with $\delta = 3.5$; *short dashed curve:* case with $\delta = 4.0$; *long dashed curve:* case with $\delta = 4.5$; *short dot-dashed curve:* case with $\delta = 5.0$; *long dot-dashed curve:* case with $\delta = 5.5$; *short-long dashed curve:* case with $\delta = 6.0$.

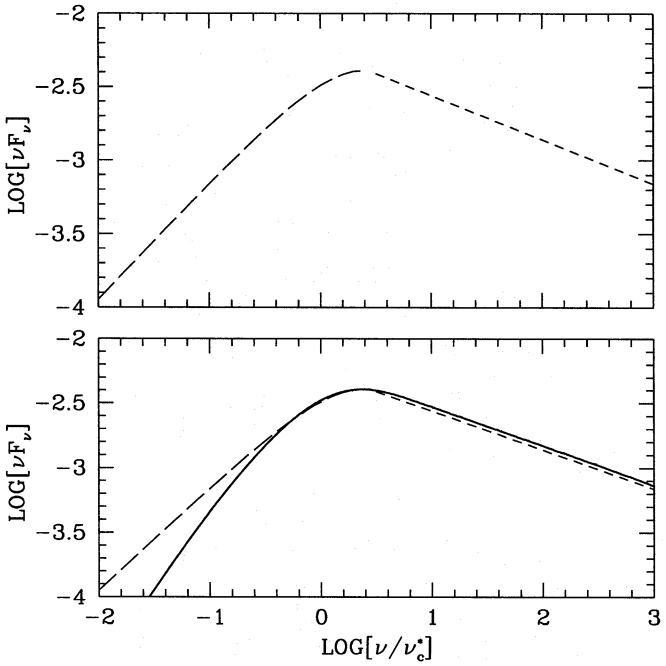

FIG. 3.—νF_ν spectrum (arbitrary units) as a function of dimensionless photon energy calculated according to the phenomenological Band's model of eq. (13) (*dashed curve*) and for the SSM (*solid curve*). *Upper plot:* dashed curve gives an example of the Band's spectral GRB model defined by a superposition of two power-law components with a smooth exponential rollover and matching imposed. Low-energy (α') and high-energy (β') power-law photon indices and critical energy E_0 have been chosen to fit the properties of GRB 910503 *near the peak of the* νF_ν spectrum. Band's model parameters in this case are $\alpha' = -1.2$, $\beta' = -2.3$, $E_0 = 3E_c = 3h\nu_c^*$. *Lower plot:* Band's model continuum (identical to the upper plot) superimposed with the calculated synchrotron shock continuum for the GRB 910503 (with $\delta = 3.8$; see Tavani 1996a). It is evident that Band's model may approximate well the continuum near the peak of the νF_ν spectrum for a proper choice of parameters. However, a discrepancy between the two models is particularly clear for energies about a decade below the peak energy. The synchrotron shock model predicts a continuum substantially below the power-law extrapolation for the α' obtained by fitting the continuum near the peak of the νF_ν spectrum. The asymptotic low-energy photon index of the SSM without attenuation or self-absorption is $\alpha' = -0.67$.

equation (13) ensures a smooth transition from the low-energy to the high-energy ranges of the emitted spectrum. We notice that if the spectral model of equation (13) is imposed to fit the high-energy part and the continuum shape near the peak of the νF_ν spectrum, Band's model is in good agreement with the SSM spectrum. However, a discrepancy between the two models appears more and more evident for photon energies typically a factor of ~ 10 below E_p. An important prediction of the SSM is therefore a discrepancy of detected emission versus the spectral model of equation (13) in the low-energy band. The discrepancy can most likely be revealed in GRBs characterized by a relatively large E_p in the MeV range. Notice that the low-energy power-law index α' of equation (13) tends to strongly overestimate the GRB emission at low energies (this point can be of crucial importance in estimating optical emission from GRBs; see § 6). Let us briefly summarize the main implications of the synchrotron shock model (Tavani 1996a).

3.1. *Determination of MHD Wind Properties from Spectral Peak Energies*

For a sufficiently large $\gamma_m \gtrsim 10\gamma_*$ (assumed in the following), the spectral shape of a single-shock episode is determined by the pair of quantities (E_c, δ), with $E_c \propto [\mathscr{D}(\Gamma, i)/(1+z)]\gamma_*^2 B_{ps}$ [for a standing shock, $\mathscr{D}(\Gamma, i) = 1$]. Note that only two parameters determine the spectral shape of (idealized) shock emission episodes.[3] By taking into account the difference between E_p and E_c, a peak energy of the νF_ν spectrum near 1 MeV corresponds to a value of the combination $[\mathscr{D}(\Gamma, i)/(1+z)]\gamma_*^2 B_{ps} \sim 4 \times 10^{13}$ cgs. A crucial consequence of the synchrotron shock model of emission is the interpretation of the GRB peak energies in the range $\sim$0.01–1 MeV in terms of the (possibly blueshifted) relativistic cyclotron energy of an MHD wind. From the observed spectral characteristics of GRBs (e.g., those of Table 1 and of published spectral analyses; see B93; Schaefer et al. 1994a), GRB relativistic winds are constrained to produce a combination of preacceleration Lorentz factors γ_* and postacceleration magnetic fields B_{ps} in the range

$$\frac{1}{[\mathscr{D}(\Gamma, i)/(1+z)]} \lesssim [\gamma_*^2 B_{ps}]_{12} \lesssim \frac{100}{[\mathscr{D}(\Gamma, i)/(1+z)]}, \quad (14)$$

where we defined $[\gamma_*^2 B_{ps}]_{12} = (\gamma_*^2 B_{ps})/10^{12}$ in cgs and neglected possible IC blueshift. Equation (14) turns out to be a fundamental property of the shock emission model of GRBs, reflecting the properties of the MHD wind and of the local magnetic field. By imposing that photons up to $\sim 10^{10}$ eV (simultaneous with the emission in the BATSE energy range) are produced and propagated from the emission region (Hurley et al. 1994), we find that the local magnetic field must satisfy the relation $B_{ps} \lesssim (10^{10}\ \mathrm{G})/(E_\gamma/10^{10}\ \mathrm{eV})\theta_\gamma^{-2}$, where E_γ is the escaping photon energy and θ_γ is the angle between the photon direction and the magnetic field. We therefore deduce that the GRB emission region is unlikely to be coincident with the site of magnetic fields expected near the surface of neutron stars with strong magnetic fields ($B_s \sim 10^{12}$ G) unless the angle θ_γ is $\sim 10^{-2}$ for the whole GRB duration. It is interesting to note that a model based on a combination of Lorentz factors and B_{ps} typical of pulsar-driven nebular environments ($B_{ps} \sim 1$–10 G, $\gamma_* \sim 10^6$–10^7) is consistent with the constraint of equation (14).

3.2. *Peak Intensity versus Duration Relation for Individual Shock Episodes (GRB Peaks)*

A general consequence of the synchrotron shock model of GRBs is a relation between the burst spectral flux $F_\nu^s \sim [\mathscr{D}(\Gamma, i)]^3 B_{ps} \mathscr{F}(\nu/[\mathscr{D}(\Gamma, i)/(1+z)]\nu_c^*)$ (eq. [12] modified by the possible effect of Doppler boosting and cosmological redshift) and the duration of single-shock episodes τ_e as determined by the synchrotron timescale in the laboratory frame

$$\tau_e \sim \tau_s \sim B_{ps}^{-2}\gamma_b^{-1}[\mathscr{D}(\Gamma, i)/(1+z)]^{-1}. \quad (15)$$

Equation (15) is valid if the observed synchrotron cooling timescale in the laboratory frame $\tau_s = \tau_s'[\mathscr{D}(\Gamma, i)/(1+z)]^{-1}$ satisfies $\tau_s \gtrsim \tau_d$, where $\tau_d \sim R_s/(c\Gamma^2)$ is the dynamical timescale of shock propagation in the laboratory frame. We notice that within the framework of the SSM *the burst emission is expected to be fainter and of longer duration for decreasing* B_{ps} and fixed γ_b. In its simplest realization, the shock model therefore predicts a relation between spectral flux (peak intensity) and duration of the shock emission

[3] However, a comparison with time-averaged GRB spectra may not reveal the underlying simple structure of the shock emission unless the bursts are dominated by well-defined emission episodes.

episode. For burst emission episodes of similar values of γ_b we have

$$I^s_{p,j} \propto \mathscr{H}(\Gamma, i, z, \gamma_*)\tau_e^{-1/2}(j) , \quad (16)$$

where $I^s_{p,j}$ denotes the peak intensity (within a given energy band) of the jth shock emission episode, $\tau_e(j)$ its duration, and $\mathscr{H}(\Gamma, i, z, \gamma_*)$ a function depending on the kinematic state of the shock front and on γ_*. The explicit form of the function $\mathscr{H}$ (and of similar $\mathscr{H}$ functions defined below) is not relevant in what follows. It is important to realize that the idealized relation of equation (16) (and similar relations given below) can be "blurred" by a variety of factors affecting the absolute normalization of peak intensities (e.g., different emission volumes and nontrivial hydrodynamical and radiative effects). However, for similar emission volumes, ensembles of GRBs characterized by similar values of the function $\mathscr{H}$ are predicted to obey the simple relation of equation (16). The relation of equation (16) might be revealed by an analysis focused on fast rise and rapid decay GRBs (FREDs), or even on different well-defined peaks *within the same GRB*.

On the other hand, if $\tau_s \lesssim \tau_d$, then the observed GRB emission is strongly dependent on the hydrodynamical interaction process, and closely spaced and blended individual shock emission episodes can be produced. In this case, the relation between the peak intensity $I^s_{p,j}$ and $\tau_e(j)$ may be complicated by poorly known dynamical effects. For the simple case of equipartition and flux conservation for spherical symmetry, $B_{ps} \sim R_s^{-2}$, we derive the relation

$$I^s_{p,j} \propto \mathscr{H}'(\Gamma, i, z, \gamma_*)\tau_e^{-2}(j) , \quad (17)$$

where $\mathscr{H}'$ is a properly defined function of shock kinematic quantities and γ_*. Note that the relations of equations (16)–(17) have meaning only for well-defined (e.g., FRED-like) pulse emission episodes of homogeneous spectral characteristics, and they do not apply in general to complex GRBs.

It is interesting to note that the effect indicated by equations (16)–(17) is qualitatively similar to the effect of cosmological time dilation (e.g., Norris et al. 1994; but also Mitrofanov et al. 1995 for different conclusions). An apparent correlated behavior between GRB peak intensities and pulse durations therefore cannot be uniquely interpreted in terms of GRB cosmological models. In principle, equations (16)–(17) can be tested for an ensemble of bright GRBs or for properly chosen GRBs showing substructure evolution and emission related to different shock emission episodes (e.g., GRBs with well separated pulses with different spectra such as GRB 911209; see Schaefer et al. 1992 and F94). The main difficulty in testing relations of the kind of equations (16)–(17) is the empirical determination of the durations of the elementary shock emission episodes. Determining τ_e can be problematic for complex contributions to the total GRB emission. Only for particularly simple GRBs (e.g., FREDs) may a relation of the kind given in equations (16)–(17) be revealed. An additional difficulty in determining τ_e may be the flux-limited nature of the sample of available GRBs. The observed durations of the pulse emission episodes may be affected by threshold effects for the GRB intensities. Complex GRBs providing a naturally selected range of burst intensities might help in this respect. If peak intensities and peak energies of the νF_ν spectrum can be determined for more than one emission episode within a complex burst, the relations of equations (16)–(17) might be tested.

3.3. *Flux versus Peak Energy Relation*

Figure 4 gives an example of synchrotron shock spectra calculated for different values of B_{ps}. The overall spectral fluxes of burst components with different magnetic fields decreases quasi-linearly with the peak intensity, i.e., in the first approximation,

$$F_{\nu,j}(E_p) \sim E^\lambda_{p,j} \sim B^\lambda_{ps,j} , \quad (18)$$

with λ an exponent that can be deduced from Figure 4, $\lambda \sim 1$, and with the label j denoting different shock emission episodes (or pulses). Equation (18) is an idealized representation of a relation $F_{\nu,j}(E_p)$ that can be complicated by a variety of effects (complex superposition of different spectral components, viewing geometry, different emission volumes, variations of γ_* within the bursts). However, the ideal quasi-linear relation of equation (18) may appreciably differ from the relation expected if the cosmological dimming effect dominates. For example, the exponent of relation, equation (18), for a purely cosmological effect (for a flat curvature universe of zero cosmological constant) satisfies $\lambda_{cosm} \simeq 2.7$. This different behavior can be testable for a proper class of GRBs (Tavani 1996b).

3.4. *Peak Energy versus Duration Relation*

For a fixed γ_*, the synchrotron model predicts also an important relation between $E_p \sim B_{ps}[\mathscr{D}(\Gamma, i)/(1+z)]$ and τ_e. As in § 3.2, we can consider the case of $\tau_s \gtrsim \tau_d$ and therefore obtain the relation valid for a single-shock emission episode j:

$$E_p(j) \propto \mathscr{H}''(\Gamma, i, z, \gamma_*)\tau_e^{-1/2}(j) . \quad (19)$$

In a way similar to § 3.2, for $\tau_s \lesssim \tau_d$ we obtain for spherical symmetry

$$E_p(j) \propto \mathscr{H}'''(\Gamma, i, z, \gamma_*)\tau_e^{-2}(j) , \quad (20)$$

where $\mathscr{H}''$ and $\mathscr{H}'''$ are properly defined functions whose exact form is not relevant here. The relations of equations

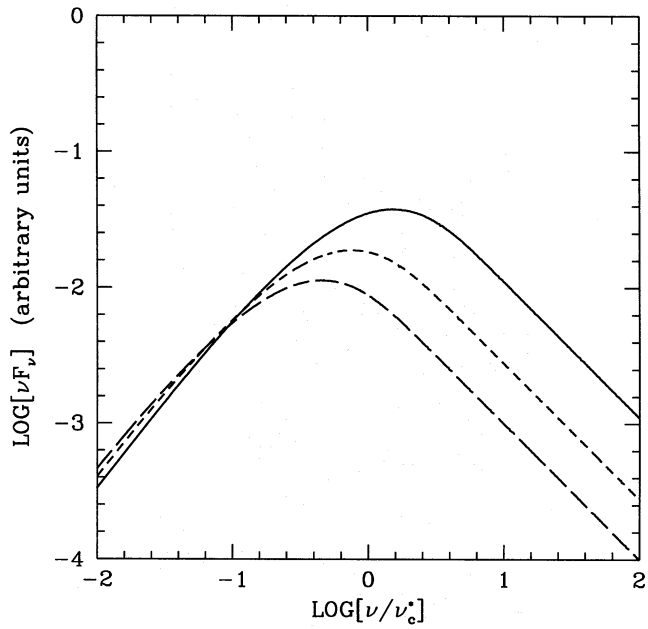

FIG. 4.—Effect of a change of magnetic field B_{ps} on the calculated νF_ν spectrum. *Solid curve:* case with $B_{ps} = 1$ (in relative units); *short-dashed curve:* case with $B_{ps} = 0.5$ (in relative units); *long-dashed curve:* case with $B_{ps} = 0.3$ (in relative units).

(19) and (20) can be established by studying the substructure (pulse) evolution *within bursts* and their corresponding spectral behavior. GRBs within a restricted range of peak intensities (or complex multipulsed GRBs) might offer the best sample to test equations (19) and (20).

3.5. *GRB Peak Duration versus Photon Energy Relation*

GRB pulse emission based on the SSM predicts a specific pattern of individual shock episode durations narrowing for increasing photon energies. In general, we expect the durations of single GRB pulses (not to be confused with the overall burst durations T_{90} or T_{50}) to be energy dependent, with longer durations expected at relatively smaller photon energies. This behavior is consistent with the prevalent observed properties of GRBs, which, for increasing photon energy, show a decrease of peak durations within bursts as first noted by Link, Epstein, & Priedhorski (1993). If the GRB pulse duration τ_e is dictated by the synchrotron timescale $\tau_s \gtrsim \tau_d$, we obtain the general relation

$$\tau_e \propto \tilde{f}(B_{\rm ps}) E^{-1/2} , \qquad (21)$$

where $\tilde{f}[B_{\rm ps}(E)]$ is a function of photon energies through the dependence on the postshock magnetic field. It is interesting to note that equation (21) is in agreement (for a constant $\tilde{f}[B_{\rm ps}(E)]$) within experimental errors with recent results based on an autocorrelation analysis of GRB light curves (Fenimore et al. 1995). The average light curve of GRB pulses shows indeed a prominent dependence on the photon energy, with a pulse duration $\tau_p \sim E^{-0.45}$ as derived by Fenimore et al. (1995).

We note here that the analysis of GRB peaks obtained with an autocorrelation method can be extended to a study of *whole* complex GRBs showing more than one well-defined peak. A study of the dependence of peak duration on photon energy for individual complex bursts can be of crucial importance in disentangling the time-variable behavior of γ_* and $B_{\rm ps}$.

3.6. *Hard-to-soft Spectral Evolution*

Complex hydrodynamical and geometrical effects can influence the spectral evolution within a single GRB. In general, there is no reason to expect that the initial value of $\mathcal{D}(\Gamma, i)[\gamma_*^2 B_{\rm ps}]_{12}$ remains constant during a shock episode or during successive episodes or pulses. Variations of $B_{\rm ps}$, δ, and Γ, expected on general grounds for hydrodynamical shocks, may lead to specific and calculable patterns of spectral changes. For fixed values of γ_* and Γ (as expected for given preshock MHD properties), hard-to-soft spectral evolution can be caused by (1) a decrease of $B_{\rm ps}$ as a consequence of postshock flow expansion, or (2) a postshock decrease of the index δ [a steepening of $n_{\rm ps}^{(3D)}(\gamma, \alpha)$] as a consequence of strong cooling processes affecting the particle energy distribution for dynamical flow times larger than τ_r (still maintaining $\tau_a \lesssim \tau_r$). Figure 2 shows the decrease of E_p as the index δ decreases. Figure 4 shows the effect of the decrease of the local magnetic field. The two effects are, in general, distinguishable, and a detailed temporal analysis of GRB spectra might reveal the dominant pattern.

3.7. *Soft-to-hard Spectral Evolution*

For an increasing value of $\mathcal{D}(\Gamma, i)[\gamma_*^2 B_{\rm ps}]_{12}$ within a burst, substantial spectral hardening is expected. Even though this effect seems observationally less favored with respect to the hard-to-soft behavior, important exceptions to the general trend are often quoted (e.g., Paciesas 1996). The considerations given in § 3.5, with proper modifications, can be applied to explain a soft-to-hard behavior. For example, an increase of the local magnetic field at the shock, or of the thermalization relativistic energy γ_*, can lead to an observable soft-to-hard spectral evolution. The functional dependence of the GRB continuum given in Figures 2 and 3 can be used to distinguish different spectral patterns. We note that hard-to-soft spectral evolution occurred during the "delayed" gamma-ray emission of GRB 940217 (Hurley et al. 1994). In this case, a hardening of the spectrum producing gamma-ray emission delayed by $\sim$1 hr with respect to the main low-energy emission can coexist with an apparent hard-to-soft spectral evolution of the main body of the emission detected by BATSE and COMPTEL (e.g., Winkler et al. 1995).

3.8. *Determination of Shock Acceleration Properties of Impulsive Events*

Detailed modeling of the shock acceleration properties of GRBs is a crucial task for future research, and an analysis of the many theoretical issues is beyond the scope of this paper. The observed time-averaged properties of bright GRBs (see § 4) are consistent with an SSM that requires very efficient particle acceleration at a shock front to explain the high-energy ($E > E_p$) emission. We can briefly point out here that theoretical calculations of radiative shocks properties for different assumptions on the MHD wind composition and structure (Γ, γ_*, σ_M, ξ, $B_{\rm ps}$) can be compared with patterns of GRB spectral evolution. Crucial to the shock acceleration hypothesis is the possibility for the acceleration to operate within the (in principle, calculable) radiation timescale of the impulsive GRB emission. For both synchrotron or IC models of the high-energy GRB emission, efficient postshock acceleration of suprathermal particles is needed to produce power-law distribution functions of indices $3 \lesssim \delta \lesssim 6$. Furthermore, GRB time variations of E_p and of the spectral continuum can be related to changes of $B_{\rm ps}$, γ_*, and δ. In principle, determining time variations of δ would be of the greatest importance for gaining information on the cooling properties of accelerated particle distributions.

3.9. *GRB Temporal Structure Reflecting the MHD Dynamics*

Ultimately, a shock model might be able to clarify the temporal structure of GRBs, a notoriously difficult problem that has defied simple interpretations. Several possibilities might arise.

Simple GRBs might be associated to morphologically single emission episodes for which a determination of burst duration τ_e and νF_ν can be obtained without ambiguities. Natural candidates of simple GRBs are bursts which show well-defined single pulses such as FREDs (e.g., F94).

Complex GRBs might result from components of heterogeneous temporal and spectral characteristics resulting from different emission or propagation properties of MHD winds interacting with the external medium. A multispike GRB with well-separated components (e.g., GRB 940217; see Winkler et al. 1995) might originate from MHD blobs ejected in different directions at the same time from the central source and with the shock emission delayed in time by propagation effects. Typical time intervals among separate pulses of $\sim$1–100 s point to a physical size of the region confining the MHD outflow of order 10^{10}–10^{12} cm.

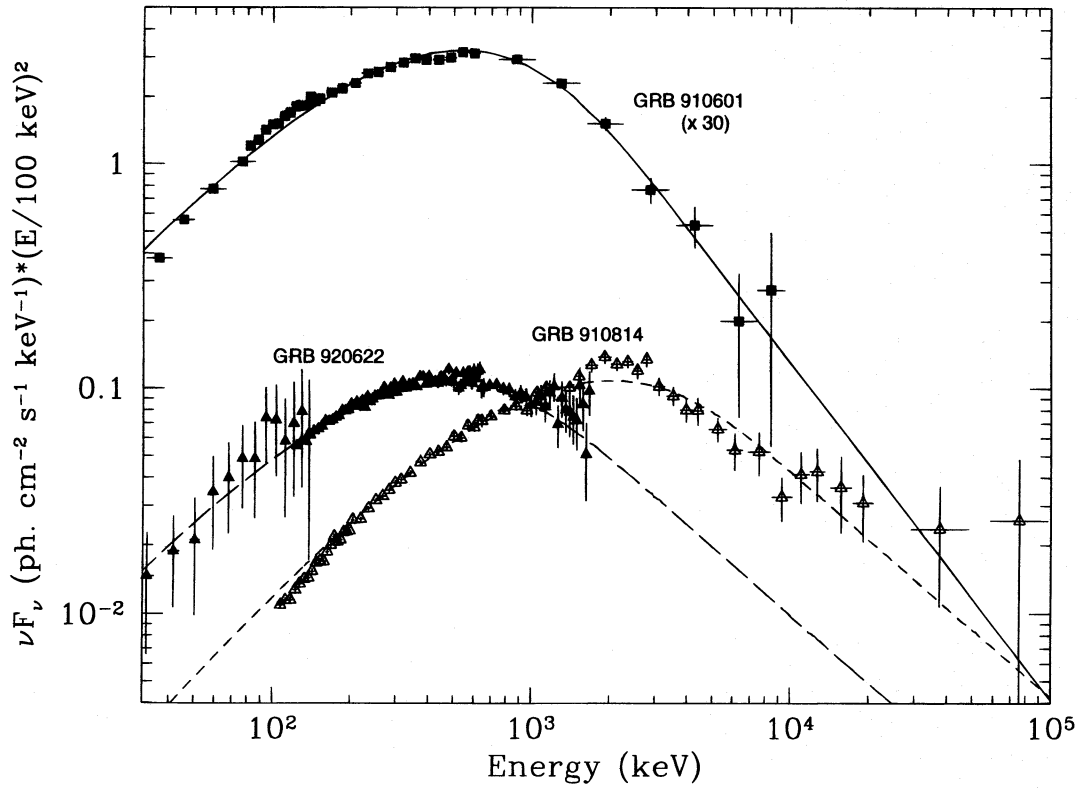

FIG. 5.—Observed composite (*CGRO* multi-instrument) νF_ν spectra of GRBs 910601, 920622, 910814, and best fit calculated νF_ν spectra (see Table 1). Data are from Schaefer et al. (1994a), Schaefer (1995), and Greiner et al. (1995). The observed GRB spectra are marginally "obliging" in the low-energy range in the sense of Fenimore et al. (1981), and the overall spectral shape is not strongly sensitive to spectral deconvolution (Schaefer et al. 1994a).

As indicated in previous sections, a combined analysis *for individual pulses* of peak intensities, peak energies, and pulse durations might clarify the details of GRB emission.

4. A COMPARISON WITH OBSERVED BRIGHT GRBS

In general, the observed spectral flux F_ν (which can be thought of as a spectral fluence function) can be ideally represented by a sum of different components

$$F_\nu = \int_0^{\tau_B} F_\nu^s(t)dt + \int_0^{\tau_B} \mathcal{K}_\nu(t)dt \,, \qquad (22)$$

where τ_B is the total burst duration, and

$$F_\nu^s(t) = \sum_j F_\nu^{s(j)}(t) \,. \qquad (23)$$

The function $\mathcal{K}_\nu$ of equation (22) represents a possible contribution to the GRB emission from precursor and/or "delayed" emission as occasionally observed in the X-ray band with a blackbody spectrum (e.g., Murakami et al. 1991; see also the 5–10 keV "excess" emission in 10%–15% of GRBs detected by BATSE; Preece et al. 1995). The sum of equation (22) extends over all different shock components (pulses) labeled by the index j. Deducing the underlying continuum emission properties from the observed spectral fluences F_ν of complex GRBs may be problematic. However, if the $F_\nu^{(j)}(t)$ values of a complex GRB spectrum were very heterogeneous among each other, it would be hard to deduce phenomenologically a quasi-universal GRB spectral shape as done with the time-averaged spectra of B93. From the relative "stability" of the GRB spectral features (see Ford et al. 1995), we infer that the components of complex GRBs are characterized by combinations of Γ, γ_*, B_{ps}, δ varying within bursts in a restricted range by a factor of $\sim$2–3. A first presentation of interesting spectral variations within single bursts was shown by Schaefer et al. (1992) for GRBs 910814, 911127, 911202, and 911209. (We note that, to our knowledge, no detailed temporal analysis of GRB spectra has yet been carried out with the use of the phenomenological B93 model of eq. [13]).

At the moment, we have to rely on available information based on time-averaged spectra. The composite multi-instrument GRB spectra summarized in Table 1 can be used for an initial preliminary comparison, even though carrying out formal spectral fits requires a proper spectral deconvolution with the detector response. It is encouraging that the synchrotron shock emission model leads to a qualitatively good agreement with all the GRB time-averaged spectra of Table 1. Let us briefly discuss some of the bright GRBs referring to the data of F94. The preliminary comparison between observed and calculated spectra presented here is meaningful because of the "nonobliging" nature[4] of the GRBs of Table 1, as checked in Schaefer et al. (1994a) in the energy range from several hundreds of keV to GeV. A possible dependence on spectral deconvolution may affect the comparison between observed and calculated spectra at low energies.

GRB 910503 is one of the brightest GRBs detected by BATSE and is characterized by a $\sim$10 s long succession of closely spaced (and possibly blended) pulse emission episodes and by a second (and much weaker) emission episode following the first one by a hiatus of $\sim$35 s (F94). No substantial spectral evolution has been detected during the first and most prominent emission episode (Schaefer et al. 1992;

[4] See Fenimore et al. (1981) for a definition of nonobliging GRB spectra, i.e., of spectra which are not strongly dependent on the spectral deconvolution in a given energy range (typically for photon energies larger than $\sim$100 keV).

Ford et al. 1995). For the first emission episode, a good agreement between the calculated and observed νF_ν spectrum is obtained for $[\gamma_*^2 B_{ps}]_{12} \sim 40/[\mathcal{D}(\Gamma, i)/(1+z)]$, and $\delta = 3.8$ (Tavani 1996a). GRB 910503 shows a substantial high-energy component extending well above 10 MeV (Schaefer et al. 1994b).

Also the combined spectrum of GRB 940217 shows a high-energy tail extending beyond 10 MeV (Hurley et al. 1994; Winkler et al. 1995). A good fit with the calculated synchrotron shock spectrum is obtained for $[\mathcal{D}(\Gamma, i)/(1+z)][\gamma_*^2 B_{ps}]_{12} \sim 25$ and $\delta \sim 4$.

On the other hand, the spectra of GRB 910601, GRB 910814, and GRB 920622 do not show prominent high-energy tails. The composite spectra of these three GRBs are given in Figure 5, together with the respective best-fit shock emission spectra. The spectrum of GRB 910814 was obtained by integrating over the whole burst duration of $\sim$40 s for a monotonically decreasing intensity (F94). The fit shown in Figure 5 is based on a single component with $[\mathcal{D}(\Gamma, i)/(1+z)][\gamma_*^2 B_{ps}]_{12} \sim 120$, which turns out to be the highest relativistic cyclotron energy for the GRBs of Table 1. A more realistic fit for GRB 910814 should be attempted by taking into account the time evolution of the spectrum, as observed by Schaefer et al. (1992).

The multipeaked emission of GRB 910601 can be fitted by a combination of synchrotron emission of two components of index $\delta \sim 6$, and of critical energies corresponding to $[\mathcal{D}(\Gamma, i)/(1+z)][\gamma_*^2 B_{ps}]_{12} \sim 24$ and $\sim$36, respectively. Figure 5 shows a simplified fit to the spectrum of GRB 910601 with $[\mathcal{D}(\Gamma, i)/(1+z)][\gamma_*^2 B_{ps}]_{12} \sim 35$ and $\delta = 6$.

Table 1 summarizes the values of $[\mathcal{D}(\Gamma, i)/(1+z)] \times [\gamma_*^2 B_{ps}]_{12}$ deduced for each GRB by an averaged fitting procedure. The physical quantities required to explain the emission of bright GRBs are remarkably constrained in a narrow range, reflecting the main characteristics of the underlying physical phenomenon.

We notice that, for the bright GRBs of Table 1, there is no sign (between 30 keV and $\sim$100 MeV) of any of the following:

1. An IC upturn of the GRB continuum at high energies or IC modification of the SSM spectral function;
2. Spectral modifications related to a possible γ-γ pair creation that would manifest themselves as a bumplike distortions of the spectral continuum;
3. Synchrotron self-absorption down to photon energies $\sim$30 keV.

All of the above points are important in constraining the physical conditions determining the radiation environment of GRBs (Tavani 1996a), and a detailed analysis of their significance will be carried out elsewhere.

5. FUTURE TESTS

A future analysis of the temporal properties of GRB spectra may clarify the nature of the GRB high-energy production mechanism. In § 3 we indicated several possible tests regarding specific relations among observable quantities. The SSM predicts a very specific two-parameter functional form that can be easily fitted as a function of time to GRBs. For GRBs of large intensity and fluence, a detailed determination of the spectral evolution will be of crucial importance. As an example, it will be interesting to determine the peak energies corresponding to the peak intensities of GRB pulses, instead of burst-averaged peak energies (E_p values).

We briefly summarize here the main work to be done in the future. It is convenient to divide the GRBs into "simple" bursts, i.e., single-pulse bursts, and "complex" bursts with complicated temporal behavior. As indicated in §§ 3.2–3.4, simple idealized relations among observed peak intensities, spectral peak energies, and pulse durations may be "blurred" by kinematic and geometric factors, in addition to intrinsic quantities such as the emission volume and burst luminosity. However, a search for correlations among I_p, E_p, and τ_e and for patterns of spectral evolution should be attempted for properly defined subclasses of GRBs. For example, for simple bursts (e.g., FREDs) the analysis indicated in § 3 can be carried out with relatively ease. Spectral evolution can be revealed *within individual bursts* for particularly strong events, and it might be possible to test the relations of § 3.2 to determine whether the emission timescale is dictated by dynamical or synchrotron/IC cooling effects. Furthermore, it will be straightforward to obtain the $I_p(E_p)$ relation by associating each peak energy of a given main pulse to the corresponding peak intensity. Simple GRBs may be characterized by single-shock emission episodes and may reveal the functional form of $I_p(E_p)$ in a clear way (see § 3.3).

For complex GRBs, the analysis may be more involved, even though in principle pulselike emission within bursts can be treated as separate contributions according to equation (22). Spectral evolution may reveal a systematic hardening of the continuum (increase of E_p) in correspondence with the onset of major pulses to be identified with elementary shock emission episodes. Furthermore, complex bursts are ideal to study the functional form of $I_p(E_p)$ independent of cosmological effects. A pulse-to-pulse variation of the emission may be due to intrinsic properties of the MHD wind/medium interaction or to geometric effects such as different emission angles of relativistic matter. In the latter case, we expect that different GRB pulses are characterized by different $\mathcal{D}$ values, and a *combined* analysis of the respective values of I_p, τ_e, and E_p might reveal this effect. For multipulsed GRBs with temporally well-separated components (e.g., GRB 940217; see Hurley et al. 1994 and Winkler et al. 1995) the analysis suggested in § 3 can be performed for each pulse separately and in combination with the others.

A main difficulty remains concerning a meaningful operational definition of the duration (τ_e) of fundamental episodes of emission associated with pulses and spikes of GRB light curves. In a flux-limited sample of GRBs, the observed durations of GRB pulses may be strongly dependent on the overall intensity of the burst, and the relations of § 3 among observable quantities may be revealed only for homogeneous samples of events within the same intensity class.

6. CONCLUSIONS

The SSM presented here provides a simple model for the GRB high-energy emission. The SSM provides a two-parameter set of spectral functions that can be used for detailed temporal studies of GRB spectra. Peak energies of νF_ν spectra are naturally produced in the observed range 100 keV $\lesssim E_p \lesssim$ 1 MeV for a combination of relativistic Lorentz factors of MHD particles and local magnetic fields $[\gamma_*^2 B_{ps}]_{12} \sim$ 1–100, modulo Doppler and cosmological redshift factors. An efficient shock acceleration mechanism is shown to be operating to produce the suprathermal high-energy tail observed in GRBs. The optically thin nature of

the nebular emission allows the propagation and escape of ~ 1 GeV photons from the shock site, in agreement with observations of bright GRBs within the EGRET field of view (Sommer et al. 1994; Hurley et al. 1994; Dingus 1995).

We showed that important relations among observable quantities (peak intensities, peak energies of the νF_ν spectrum, τ_e durations) may be revealed by a combined temporal and spectral analysis of the GRB emission. An intrinsic spread of burst luminosities as well as geometric and kinematic factors may "blur" correlated behaviors of observables as discussed in § 3. Purely cosmological effects might be distinguished from B-driven features of the emission for a subclass of GRBs. Future studies of GRBs might identify homogeneous classes of bursts and search for correlations predicted by the SSM.

In general, the total duration of GRBs (e.g., T_{90} extensively used in GRB studies) does not simply relate to any of the relevant physical processes involved in GRBs (radiative cooling or hydrodynamical processes). A more meaningful timescale is suggested here to be associated with the (possibly time-dilated) cooling timescale of shock-accelerated particles. We tentatively suggest that the cooling timescale is associated with the duration of pulse emission episodes characterizing the majority of GRB light curves. The precise operational definition of the pulse durations (τ_e) introduced in § 3 may be problematic for a flux-limited sample of GRBs. A homogeneous (in peak intensity) subclass of GRBs can be considered to study the predicted correlations of § 3.

The SSM naturally solves the "X-ray paucity" problem of GRBs (e.g., Laros et al. 1984; Higdon & Lingenfelter 1990; Harding 1991) for (possibly blueshifted) relativistic cyclotron energies in the 100 keV–1 MeV range. The typical observed ratio of fluences S in the X-ray and soft γ-ray bands is $S_X/S_\gamma \sim 10^{-2}$ (Laros et al. 1984). The X-ray paucity constraint is naturally explained in terms of the behavior expected if the synchrotron emission dominates $S_X/S_\gamma \sim (\nu_X/\nu_p)^{4/3}$, with $h\nu_p \gtrsim 100$ keV and $h\nu_X \sim 1$–10 keV (h being Planck's constant). This is a general property of the SSM, and is independent of the Galactic or cosmological nature of the GRB sources. It is worth noticing that a possible contribution from an X-ray precursor or tail represented by the function $\mathcal{K}_\nu$ of equation (22) (Murakami et al. 1991; Preece et al. 1995) does not appear to dominate the emission in the X-ray band. This additional X-ray contribution might produce an observable low-energy tail in the UV band possibly detectable by High Energy Transient Experiment (HETE; Vanderspek et al. 1995). If the synchrotron shock continuum dominates the emission, the predicted ratio of fluences of the UV and soft γ-ray bands for no self-absorption is $S_{UV}/S_\gamma \sim (\nu_{UV}/\nu_p)^{4/3} \sim 5 \times 10^{-6}$ for $h\nu_{UV} = 10$ eV and $h\nu_p = 100$ keV. The UV low energy tail of the synchrotron emission might be below the HETE detection threshold even for GRBs of large fluence ($S_\gamma \sim 10^{-3}$ ergs cm^{-2} s^{-1}) and relatively low values of E_p. In the absence of additional spectral components, no self-absorbed optical fluxes are predicted by the SSM with fluence ratios larger than $S_0/S_\gamma \sim (\nu_0/\nu_p)^{4/3} \sim 5 \times 10^{-7}$, for $h\nu_0 = 2$ eV, and $h\nu_p = 100$ keV.

Future studies of time-resolved GRB spectral properties will be of crucial importance for clarifying the nature of the GRB high-energy emission. The synchrotron shock model can be thoroughly tested for a broad sample of GRBs of different complexity.

The author wishes to thank B. Schaefer, J. Greiner, and C. Winkler for important exchange of information on GRB composite spectra, and R. Preece, D. Band, B. Dingus, and L. Hanlon for discussions. Research supported by NASA through grant NAG 5-2729. This work is Columbia Astrophysics Laboratory contribution no. 592.

REFERENCES

Arons, J. 1991, in IAU Colloq. 128, The Magnetospheric Structure and Emission Mechanisms of Radio Pulsars, ed. J. A. Gil & J. M. Rankin (Ziolona Góra: Pedagogical Univ. Press), 56
Band, D., et al. 1993, ApJ, 413, 281 (B93)
Begelman, M. C., Blandford, R. D., & Rees, M. J. 1984, Rev. Mod. Phys., 56, 265
Begelman, M. C., & Kirk, J. G. 1990, ApJ, 353, 66
Chiueh, T., Li, Z.-Y., & Begelman M. C. 1991, ApJ, 377, 462
Dingus, B. 1995, Ap&SS, 231, 187
Fenimore, E. E., Klebesadel, R. W., & Laros, J. G. 1981, in Ganıma-Ray Astronomy in Perspective of Future Experiments (New York: Pergamon), 201
Fenimore, E. E., Zand, J. J. M., Norris, J. P., Bonnell, J. T., & Nemiroff, R. J. 1995, ApJ, 448, L101
Fichtel, C. 1996, in Proc. Third Compton Symp., A&AS, in press
Fishman, G. J., et al. 1994, ApJS, 92, 229 (F94)
Ford, L. A., et al. 1995, ApJ, 439, 307
Greiner, J., et al. 1995, A&A, 302, 121
Hakkila, J., et al. 1994, ApJ, 422, 659
Hanlon, L. O., et al. 1994, A&A, 285, 161
Harding, A. K. 1991, Phys. Rep., 206, 327
Hartmann, D. H., Briggs, M. S., & Mannheim, K. 1996, in AIP Conf. Proc., Third Huntsville Symp. on Gamma-Ray Bursts, ed. C. Kouveliotou, M. Briggs, & G. J. Fishınan (New York: AIP), in press
Hester, J., et al. 1995, ApJ, 448, 240
Higdon, J. C., & Lingenfelter, R. E. 1990, ARA&A, 28 401
Hjellming, R. M., & Rupen, M. P. 1995, Nature, 375, 464
Hoshino, M., et al. 1992, ApJ, 390, 454
Hurley, K., et al. 1994, Nature, 372, 652
Katz, J. 1994, ApJ, 432, L107
Kennel, C. F., & Coroniti, F. V. 1984, ApJ, 283, 694
Kouveliotou, C. 1992, in Proc. Compton Observatory Science Workshop, ed. C. Shrader, N. Gehrels, & B. Dennis (NASA CP-3137), 61
Jones, F. C., & Ellison, D. C. 1991, Space Sci. Rev., 58, 259
Jones, T. W., & Hardee, P. E. 1979, ApJ, 228, 268
Laros, J. G., et al. 1984, ApJ, 286, 681
Link, B., Epstein, R. I., & Priedhorski, W. C. 1993, ApJ, 408, L81
Meegan, C., et al. 1992, Nature, 355, 143
———. 1996, 3rd BATSE catalog, ApJ, submitted
Mészáros, P., Laguna, P., & Rees, M. J. 1993, ApJ, 415, 181
Mészáros, P., & Rees, M. J. 1993, ApJ, 405, 278
Mészáros, P., Rees, M. J., & Papathanassiou, H. 1994, ApJ, 432, 181
Mirabel, I. F., & Rodriguez, L. F. 1994, Nature, 371, 46
Mitrofanov, I., et al. 1995, Ap&SS, 231, 103
Murakami, T., et al. 1991, Nature, 350, 592
Narayan, R., Paczyński, B., & Piran, T. 1992, ApJ, 395, L83
Norris, J. P., et al. 1994, ApJ, 424, 540
Pacholczyk, A. G. 1969, Radio Astrophysics (San Francisco: Freeman)
Paciesas, W. 1996, in Proc. Third *Compton GRO* Symposium, A&AS, in press
Paczyński, B. 1990, ApJ, 363, 218
Piran, T., Shemi, A., & Narayan, R. 1993, MNRAS, 263, 861
Preece, R., et al. 1995, Ap&SS, 231, 207
Rees, M. J., & Meszaros, P. 1992, MNRAS, 258, 41P
Schaefer, B. E. 1995, private conımunication
Schaefer, B. E., et al. 1992, ApJ, 393, L51
———. 1994a, ApJS, 92, 285
———. 1994b, in AIP Conf. Proc. 307, Gamma-Ray Bursts, ed. G. J. Fishman, J. J. Brainerd, & K. Hurley (New York: AIP), 271
Shemi, A., & Piran, T. 1990, ApJ, 365, L55
Sommer, M., et al. 1994, ApJ, 422, L63
Tavani, M. 1994, ApJ, 431, L83
———. 1995, Ap&SS, 231, 181
———. 1996a, Phys. Rev. Lett., 76, 3478
———. 1996b, in AIP Conf. Proc., Third Huntsville Symp. on Gamma-Ray Bursts, ed. C. Kouveliotou, M. Briggs, & G. J. Fishman (New York: AIP), in press
Tavani, M., & Arons, J. 1996, ApJ, submitted
Vanderspek, R., et al. 1995, Ap&SS, 231, 479
Winkler, C., et al. 1995, A&A, 302, 765